Available online at www.sciencedirect.com
SCIENCE DIRECT®
Pergamon
International Journal of Machine Tools & Manufacture 43 (2003) 1001–1014
INTERNATIONAL JOURNAL OF MACHINE TOOLS & MANUFACTURE
DESIGN, RESEARCH AND APPLICATION

# Machining contour errors as ensembles of cutting, feeding and machine structure effects

Yuan-Ming Cheng, Jih-Hua Chin *

*Department of Mechanical Engineering, National Chiao Tung University, Hsinchu 300, Taiwan, ROC*

Received 21 October 2002; received in revised form 7 March 2003; accepted 14 March 2003

**Abstract**

CNC machining has been studied from the perspective of either cutting or feeding. However, machining quality is the outcome of both of these processes. This work investigates the contour errors of a complete CNC machine system. A system model is developed to cover all groups of functions, including trajectory planning, trajectory tracking, cutting process and machine structure. Analysis results reveal the limitations of traditional studies. The dependence of contour errors on trajectory curvature, feed-rate, cutting depth and tracking control is investigated as well. A new model of CNC machining is developed.


*Keywords:* Machining; Contour error; Structure; Tracking; Ensemble

## 1. Introduction

The quality of a workpiece, in terms of either surface finish or contour accuracy, is the overall outcome of cutting, feeding and machine structure dynamics. Surface finish has normally been studied from the perspective of cutting dynamics while contour accuracy has typically been studied from the perspective of tracking control, but both need to be considered from the combined perspective of cutting, feeding and machine structure. This is especially true for milling, because milling is the primary machining process that produces profiles or contours on workpieces.

Cutting force is the main factor in cutting process dynamics. Martelloti [1] and Tlusty [2] performed a fundamental analysis and modeled cutting force for milling. Cutting force models for end milling [3,4], face milling [5,6] and ball end milling [7] have been developed based upon various tool geometries, work materials, and other factors. These cutting force models help to predict forces and determine optimal cutting parameters.

The phenomenon of the excitation of cutting force on the machine structure is an essential topic for analysis in understanding machining quality. Sutherland and DeVor [8], Montgomery and Altintas [9], Budak and Altintas [10], and Ismail et al. [11] examined cutting process dynamics with reference to the combined cutting force and machine tool spindle.

Surface finish can be predicted by consideration to this depth. However, one factor has remained unexamined—the deviation due to feeding. Fig. 1(a) shows a milling tool in cutting. The consideration of tool (cutting force) and the machine structure (represented by spindle) equals to an assumption of perfect feeding. Fig. 1(b) depicts real circumstances in which feeding (tracking) errors are also involved in undulating the uncut chip and, thereby, affecting the cutting dynamics.

The development of tracking techniques has been accounted for by a large effort in feeding control. Since the first studies of two-dimensional feedback by Sarachik and Ragazzini [12], cross-coupled structures have been constantly improved and evolved into state-of-the-art algorithms for feeding control. Koren [13,14] proposed a symmetrical cross-coupled system, which improved the contour accuracy of a two-axis system. Kulkarni and Srinivasan [15] presented cross-coupled compensation for a multi-axis feeding system.

The trend toward high-speed milling has ushered in high-speed feeding. Chin and Lin [16] proposed pre-compensated cross-coupling, which provides good per-

* Corresponding author. Fax: +886-3-5727485.
*E-mail address:* jhchin@mail.nctu.edu.tw (J.-H. Chin).

0890-6955/03/$ - see front matter © 2003 Elsevier Science Ltd. All rights reserved.
doi:10.1016/S0890-6955(03)00093-2

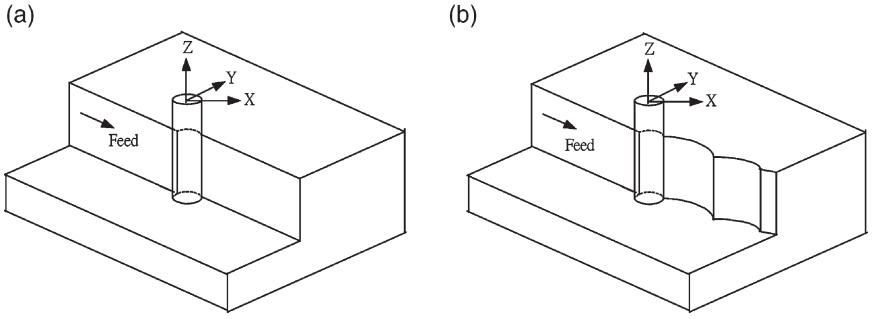


Fig. 1. Cutting with (a) perfect feeding, (b) real feeding.

formance at a high feeding speed. Cutting dynamics, tracking control and contour accuracy acquire new aspects of investigation in the era of high-speed cutting. Erkorkmaz and Altintas [17] and Mei et al. [18] investigated the effects of friction in high-speed feeding and cutting.

Earlier research on contour accuracy has been deficient in taking only selected factors into consideration. The purpose of this work is to examine accuracy of contours, by considering contours as an ensemble of cutting, feeding and machine structure dynamics.

## 2. System for CNC machining

Trajectory planning, trajectory tracking, the cutting process and machine structure dynamics constitute the four fundamental groups of functions in modern CNC machining. Conventionally, studies have addressed these groups, with reference to feeding and cutting. In reality, however, these are integral parts of a complete CNC machining system, as depicted in Fig. 2.

In Fig. 2, the trajectory data $V_x$,$V_y$,$X_f$,$Y_f$ are outputs of trajectory planning. Trajectory tracking is shown as a cross-coupled pre-compensation control. The tracking results, the actual positions of the workpiece/tool tip, affect the development of the cutting force, and the cutting force excites the machine structure (mostly represented by the spindle), which in turn modulates the congruent point of the workpiece/tool tip.

The functional blocks in Fig. 2 will be discussed to examine the contour error as an ensemble of cutting, feeding and machine structural effects.

### 2.1. Tracking control

Many tracking control schemes have been proposed to enable manufacturing workpiece with more precision. Fig. 3 shows the structure of the cross-coupled pre-compensation method (CCPM) [16], in which a velocity pre-compensation gain $K_v$ is used to generate a far feedback pre-compensation loop. Cross-coupling compensation feedback loops are formed with gains $K_{\varepsilon X}$ and $K_{\varepsilon Y}$. If $K_v$, $K_{\varepsilon X}$ and $K_{\varepsilon Y}$ are set to zero, then the system reduces to an uncoupled tracking control system (US). If both $K_{\varepsilon X}$ and $K_{\varepsilon Y}$ are set to zero, while the $K_v$-loop is main-

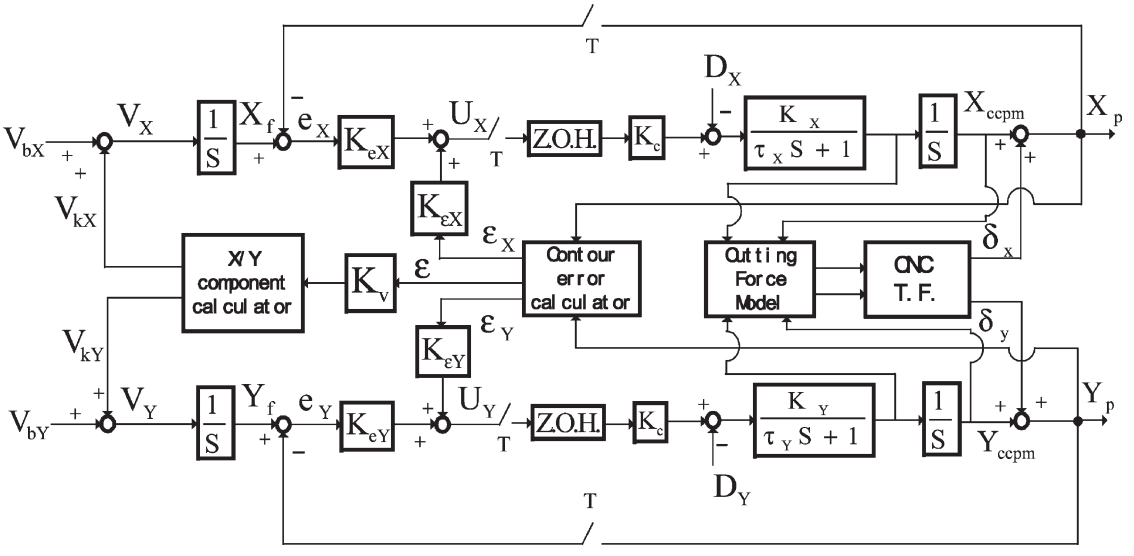


Fig. 2. The structure of CNC machining.

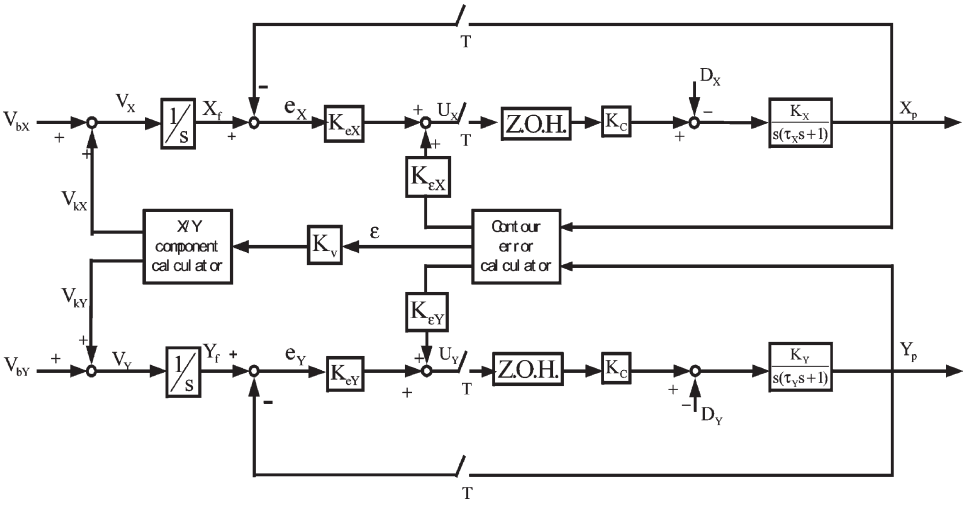


Fig. 3. Cross-coupled pre-compensation control (CCPM) for tracking.

Table 1
Four tracking controls deduced from Fig. 3

| | $K_v$ | $K_{zx}$ | $K_{zy}$ |
|---|---|---|---|
| US | 0 | 0 | 0 |
| PM | Non-zero gain | 0 | 0 |
| CCS | 0 | Non-zero gain | Non-zero gain |
| CCPM | Non-zero gain | Non-zero gain | Non-zero gain |

tained, then the system is the path pre-compensation control (PM). On the other hand, if the $K_v$-loop is omitted, while the loops formed with $K_{\varepsilon X}$ and $K_{\varepsilon Y}$ are maintained, then the system becomes a typical cross-coupled tracking control system (CCS). Table 1 lists different variations of the structure in Fig. 3.

One feature of CCPM is that it implements specific trajectory strategy for each target trajectory. For example, for linear feeding along the path $\overline{OB}$ in Fig. 4, the contour error $\varepsilon$, which is the shortest distance between the actual tool position, $P$, and the target path,

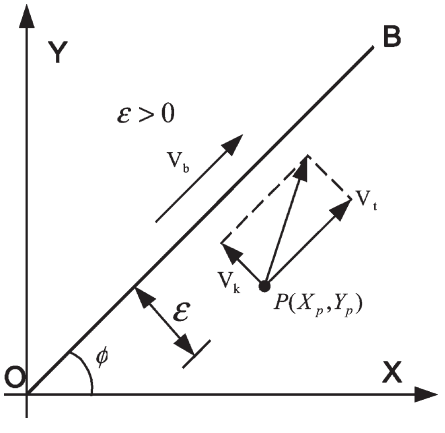


Fig. 4. Linear tracking using CCPM.

shall be found in order to form compensation toward the path. This velocity compensation $\vec{V}_k$ ($V_k = K_v\varepsilon$) tries to "push" the tool back onto the target path in a forward-looking sense. After the velocity is modified, the tool takes on a velocity vector, which is a vector combination of the required tangential velocity $\vec{V}_t$ and the modifying velocity $\vec{V}_k$ triggered by the contour error. The components of the "pre-compensated" velocity are as follows:

$$V_x = V_{tx} + V_{kx} = V_t\cos\phi - K_v\varepsilon\sin\phi, \text{ and} \quad (1)$$

$$V_y = V_{ty} + V_{ky} = V_t\sin\phi + K_v\varepsilon\cos\phi, \quad (2)$$

where $\vec{V}_t = V_b\hat{t}$ and $\phi$ is the angle between the path and the inertial coordinate $x$.

The new reference position $(X_f,Y_f)$, the desired position, is generated by considering the velocity

$$X_f(n) = X_f(n-1) + TV_x, \text{ and} \quad (3)$$

$$Y_f(n) = Y_f(n-1) + TV_y. \quad (4)$$

These equations are in fact the path generator rather than the more passive path interpolator in conventional CNC trajectory planning. The components of the position error are the differences between the components of the monitored actual position $(X_p,Y_p)$ and those of the desired position $(X_f,Y_f)$:

$$e_x(n) = e_x(n-1) + [X_f(n) - X_p(n)], \text{ and} \quad (5)$$

$$e_y(n) = e_y(n-1) + [Y_f(n) - Y_p(n)]. \quad (6)$$

CCPM requires different algorithms to calculate the contour error $\varepsilon$ for different trajectories. The following is for a linear trajectory:

$$\varepsilon = X_p\sin\phi - Y_p\cos\phi \quad (7)$$

$$\varepsilon_X = -\varepsilon\sin\phi \quad (8)$$

$$\varepsilon_Y = \varepsilon\cos\phi \quad (9)$$

Fig. 3 reveals that the control signals for the feeding

drives take care of both the position error and the contour error.

$$U_x = K_{ex}e_x + K_{\varepsilon x}\varepsilon_x \tag{10}$$

$$U_y = K_{ey}e_Y + K_{\varepsilon y}\varepsilon_y \tag{11}$$

A different algorithm is required to calculate the contour error and the velocity compensation for a circular trajectory. Fig. 5 shows a circular trajectory, in which the arc $A\bar{B}C$ is the target contour of machining; $P$ is the actual tool position, and $R$ is the distance between $P$ and the origin of the coordinates. The contour error $\varepsilon$, which is the shortest distance between the actual position and the target trajectory, is calculated from

$$\varepsilon = R - R_p = R - (X_p^2 + Y_p^2)^{\frac{1}{2}}, \tag{12}$$

$$\varepsilon_x = \varepsilon \times \left(\frac{X_p}{R}\right), \text{ and} \tag{13}$$

$$\varepsilon_y = \varepsilon \times \left(\frac{Y_p}{R}\right). \tag{14}$$

After velocity pre-compensation, the tool adopts a velocity vector, which is the vector combination of the original tangential velocity $\vec{V}_t$ along the trajectory and the modifying velocity $\vec{V}_k$, which tries to push the tool back onto the right trajectory:

$$V_x = V_{bx} + V_{kx} = -V_b\left(\frac{Y_p}{R}\right) + K_v\varepsilon\left(\frac{X_p}{R}\right), \text{ and} \tag{15}$$

$$V_y = V_{by} + V_{ky} = V_b\left(\frac{X_p}{R}\right) + K_v\varepsilon\left(\frac{Y_p}{R}\right). \tag{16}$$

The control signals $U_X$ and $U_Y$ sent to the feeding drives are the same as those in Eqs. (10) and (11).

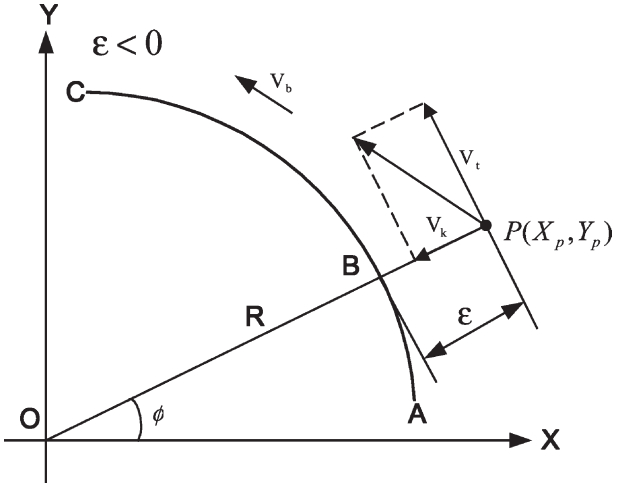


Fig. 5. Circular tracking using CCPM.

### 2.2. Cutting dynamics

The formation of cutting force and the excitation of the machine structure by the cutting force contribute to the cutting dynamics.

#### 2.2.1. Formation of cutting force

Tlusty [2] developed a cutting force model by axially splitting the cutting depth $L$ of the cutting tool into $n$ sections, generating $(n+1)$ cutting elements of elemental height dz, as shown in Fig. 6. Each cutting element was treated as performing an independent cutting process. The cutting force was the vector sum of all elemental cutting forces.

Fig. 6 shows the geometry of the cutting edges. The cutting force on the cutting edge can be decomposed into the tangential component $dF_t$ and the radial component $dF_r$:

$$dF_{tij}(t) = K_t \cdot dz \cdot h_{ij}(t) \tag{17}$$

$$dF_{rij}(t) = K_r \cdot dF_{tij}(t) \tag{18}$$

where the specific cutting forces are expressed by,

$$K_t = K_T h_a^{-p} \tag{19}$$

$$K_r = K_R h_a^{-q}, \tag{20}$$

and

$$h_a = \frac{c}{2\pi} \tag{21}$$

The subscript $i$ refers to the cutting edge; $j$ represents the cutting element. The empirical coefficients $K_T$, $K_R$, $p$ and $q$ have to do with materials and can be determined experimentally [3]. The term $h_{ij}(t)$ in Eqs. (17) and (18) are the so-called "uncut chip thickness", which depend on the feed per tooth $c$ and the instantaneous angle between the respective cutting element and the moving coordinate, $y$:

$$h_{ij}(t) = c \cdot \sin\phi_{ij}(t) \tag{22}$$

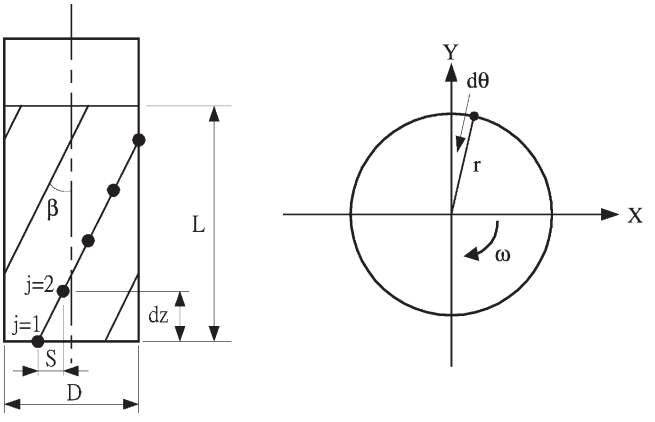


Fig. 6. Tool geometry.

$$\phi_{ij}(t) = \theta(t) + i\cdot\phi_p - (j-1)\cdot d\theta \tag{23}$$

$$\theta(t) = \omega\cdot t \tag{24}$$

where $\omega$ denotes the rpm of the spindle and $d\theta$ is the circumferential angle projected by the cutting edge, as shown in Fig. 6. The pitch angel $\phi_p$ can be calculated as $\phi_p = 2\pi/m$, where $m$ is the number of cutting edges. The corresponding arc length is

$$s = r\cdot d\theta \Rightarrow d\theta = \frac{\tan\beta}{r}\cdot dz \tag{25}$$

where $\beta$ is the spiral angle of the tool, and $r$ is the radius of the tool.

The elemental cutting forces can be transformed into moving coordinates $x$–$y$:

$$\begin{bmatrix} dF_{xij}(t) \\ dF_{yij}(t) \end{bmatrix} = \begin{bmatrix} \cos\phi_{ij}(t) & \sin\phi_{ij}(t) \\ -\sin\phi_{ij}(t) & \cos\phi_{ij}(t) \end{bmatrix} \begin{bmatrix} dF_{tij}(t) \\ dF_{rij}(t) \end{bmatrix} \tag{26}$$

which can be summed to form the total cutting forces:

$$\begin{aligned} F_x(t) &= \sum_{i=0}^{m-1} \sum_{j=1}^{n+1} dF_{xij}(t), \\ F_y(t) &= \sum_{i=0}^{m-1} \sum_{j=1}^{n+1} dF_{yij}(t), \end{aligned} \tag{27}$$

Eqs. (17)–(27) were used to determine the cutting forces in machining.

### 2.2.2. Machine structure

A complete dynamic model of cutting process involves cutting forces and the transfer function of the machine structure. Two structures importantly contribute to the cutting dynamics—the spindle system (Fig. 7) and the feeding system (Fig. 8). Since an accurate model of these non-linear, multi-DOF structural systems is highly complicated, a simplified approach was adopted. The spindle and feeding table were modeled by a second order system in the $x$- and $y$-directions.

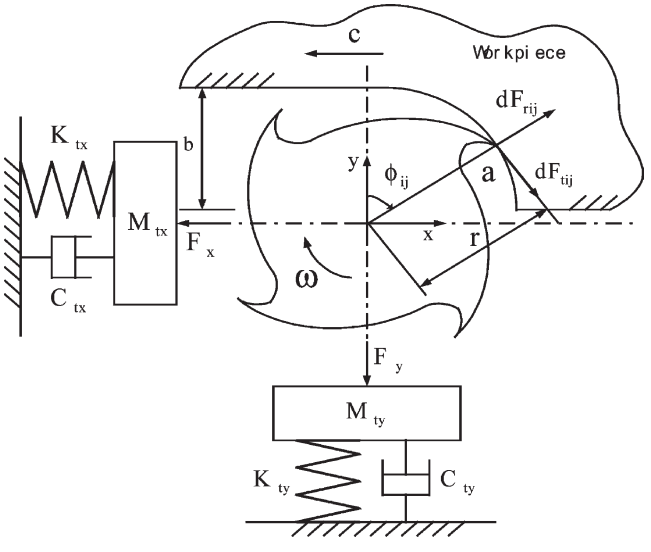


Fig. 7. Dynamic model for tool/spindle system.

The tool/spindle system was modeled by the following second order system:

$$\begin{aligned} M_{tx}\ddot{X}_t(t) + C_{tx}\dot{X}_t(t) + K_{tx}X_t(t) &= F_x(t) \\ M_{ty}\ddot{Y}_t(t) + C_{ty}\dot{Y}_t(t) + K_{ty}Y_t(t) &= F_y(t) \end{aligned}, \tag{28}$$

and the feeding table was modeled by another second order system:

$$\begin{aligned} M_{wx}\ddot{X}_w(t) + C_{wx}\dot{X}_w(t) + K_{wx}X_w(t) &= F_x(t) \\ M_{wy}\ddot{Y}_w(t) + C_{wy}\dot{Y}_w(t) + K_{wy}Y_w(t) &= F_y(t) \end{aligned}. \tag{29}$$

where $M_t$, $C_t$ and $K_t$ represent tool mass, damping and stiffness, respectively; $X_t$ and $Y_t$ are the displacements of the tool in $x$- and $y$-directions, respectively, and $F(t)$ is the cutting force. $M_w$, $C_w$ and $K_w$ are table mass, damping and stiffness, respectively. The parameters in the models were empirically determined.

## 3. Experiments

The purposes of the experiments are (1) to calibrate the cutting force model and (2) to identify the spindle–tool dynamics and the table transfer function.

### 3.1. Experiments on cutting dynamics

Fig. 9 shows experiments on cutting dynamics. The machine tool is a DYNA DM2800 CNC table milling machine. Workpieces are made of aluminum alloy Al6061, the cutter is a four-edge high-speed steel milling tool with a diameter of 10 mm. Cutting forces were measured by a 260A force cell and recorded by an HP3560A dynamic analyzer. The table displacements were monitored by optical scales and recorded by an ADC-Card ENC9266.

Cutting conditions were set as follows; spindle speed 1200 rpm, feed-rate 600 mm/min, axial depth of cut 1 mm, and radial width of cut 5 mm. Fig. 10 shows the measured and predicted cutting forces in the $x$- and $y$-directions when cutting is performed in the $x$-direction. The dotted line (blue) represents the measured cutting force, and the solid line (red) represents the cutting force produced by the cutting force model. The cutting force model is calibrated close to the actual cutting force formation mechanism. Hence, the cutting force model is useful in further investigation.

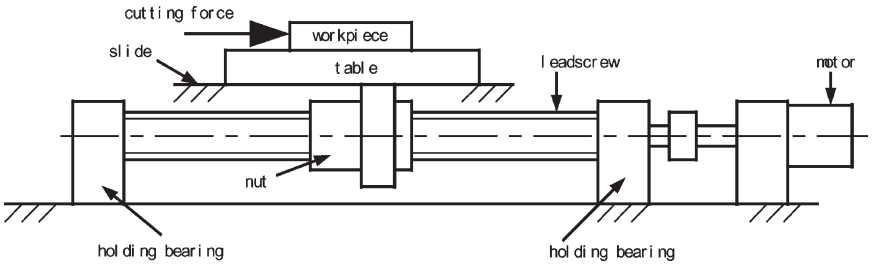


Fig. 8. Feeding system.

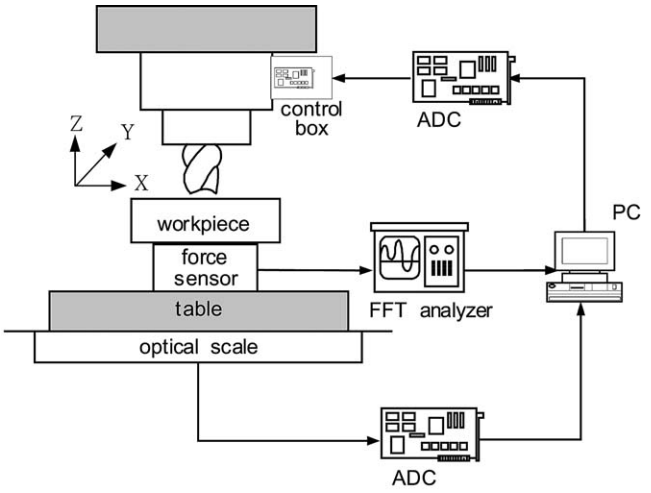


Fig. 9. Experimental arrangement for cutting dynamics.

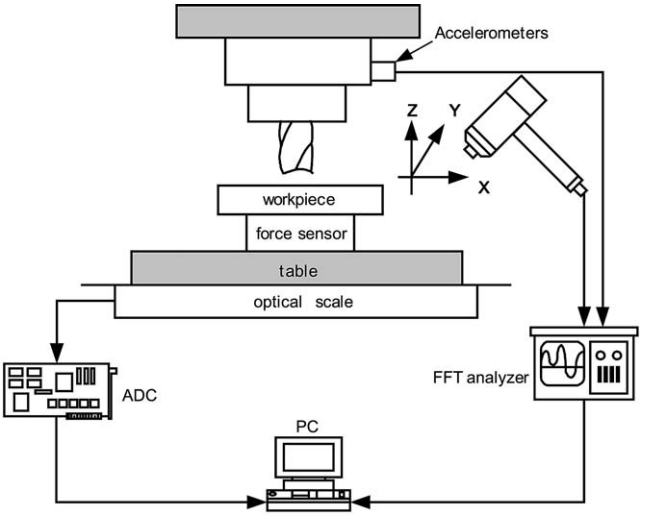


Fig. 11. Experiments on structure characteristics.

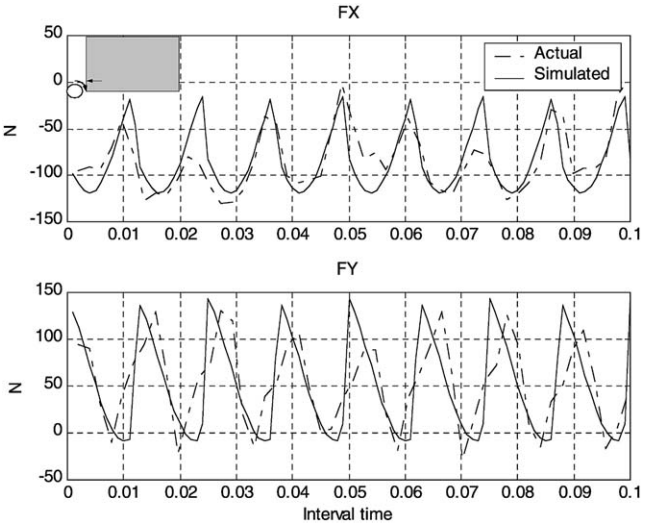


Fig. 10. Comparison of experimental and simulated cutting forces.

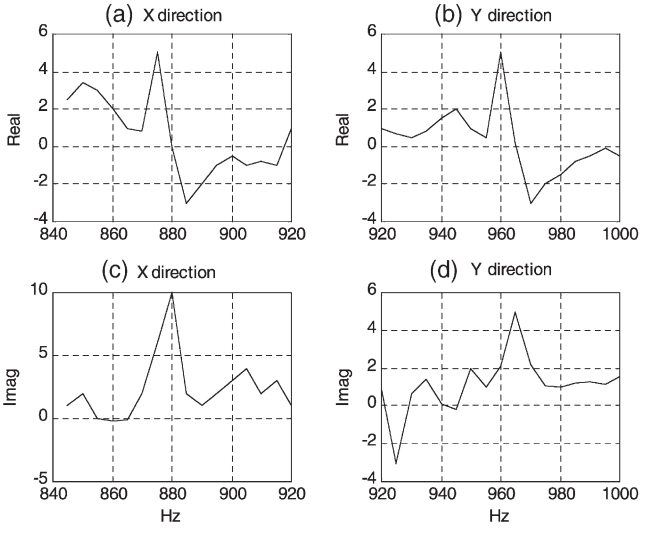


Fig. 12. Frequency response of spindle–tool.

### 3.2. Experiments on structural dynamics

#### 3.2.1. Spindle–tool dynamics

The system parameters of the spindle–tool and the table transfer function were obtained by performing the experiments presented in Fig. 11. The spindle–tool was excited by a hammer and the signals from accelerometers were collected and analyzed by an FFT analyzer. Fig. 12 plots the frequency response, the real part of which was zero and the imaginary part of which was maximal at 880 Hz in the *x*-direction and at 965 Hz in

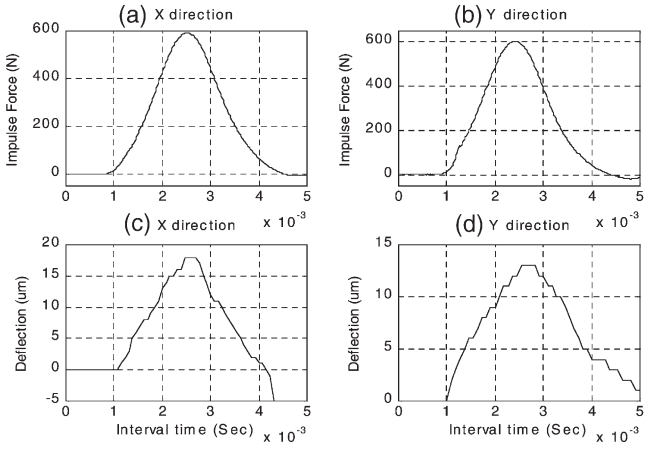


Fig. 13. Impulse forces vs. deflection of table.

the *y*-direction. The system parameters were obtained by the quadrature method [19]:

$$M_{tx} = M_{ty} = 0.12 \text{ kg}$$

$$\zeta_{tx} = \zeta_{ty} = 0.013 \left(\zeta = C/2\sqrt{K/M}\right)$$

$$K_{tx} = 9.12{*}10^5 \text{ N/m}, \quad K_{ty} = 1.1{*}10^6 \text{ N/m},$$

$$H_{tx}(s) = \frac{X_{tx}(s)}{F_x(s)} = \frac{8.33}{S^2 + 22.88S + 774400} \tag{30}$$

$$H_{ty}(s) = \frac{X_{ty}(s)}{F_y(s)} = \frac{8.33}{S^2 + 25.1S + 931225} \tag{31}$$

*3.2.2. Table structure*

Similarly, the table was excited by a hammer and the signals were monitored by an optical scale and collected by an ENC9266. Fig. 13 shows the impulse force of a hammer and the corresponding deflection of the table in the *x*- and *y*-directions as analyzed by an HP3560A dynamic analyzer.

The table transfer function was identified by the ARX model, and in the *x*- and *y*-directions, the function was as follows.

$$H_{wx}(s) = \frac{450.4S + 65220}{S^2 + 2155S + 566200} \tag{32}$$

$$H_{wy}(s) \frac{-15.83S - 41680}{S^2 + 1845S + 394300} \tag{33}$$

The transfer function can be confirmed by applying the measured excitation force to the identified transfer function and comparing the output with that measured directly from the machine, as in Fig. 14.

Applying the empirical cutting forces to the identified transfer function yields table deflections useful in simulation. Fig. 15 compares the measured table displacements (blue) with the simulated displacements, generated by applying forces in Fig. 10 to the transfer function (red). Fig. 14 shows that the simulated table deflections tend to be conservative, giving reason for caution, because the real situation might be worse than that predicted by studies based on the constructed system model.

## 4. Simulations and discussion

Complete CNC machining, as proposed in Fig. 2, was simulated with the following complete groups of functions—trajectory planning (Eqs. (1) and (2) for linear trajectory, Eqs. (15) and (16) for circular trajectory), trajectory tracking (CCPM, Eqs. (10) and (11)), the empirical cutting force model (Eqs. (17)–(27)), the empirical spindle–tool structure (Eqs. (30) and (31)), the empirical table structure (Eqs. (32) and (33)) and for the purpose of comparison, feeding drive parameters from Koren [14], $\tau_x = 0.04$, $\tau_y = 0.045$, $Kc{\cdot}Kx = 10.3$ and $Kc{\cdot}Ky = 10$.

The gains used in the controls were determined following the method of Chin and Lin [16] and are listed in Tables 2 and 3.

Koren [14] addressed tracking technology, and made the gains variable to cope with various conditions [14], but without straightforward consideration of all functions of CNC machining, unknown and uncontrolled error sources remain, as can be observed in Fig. 16,

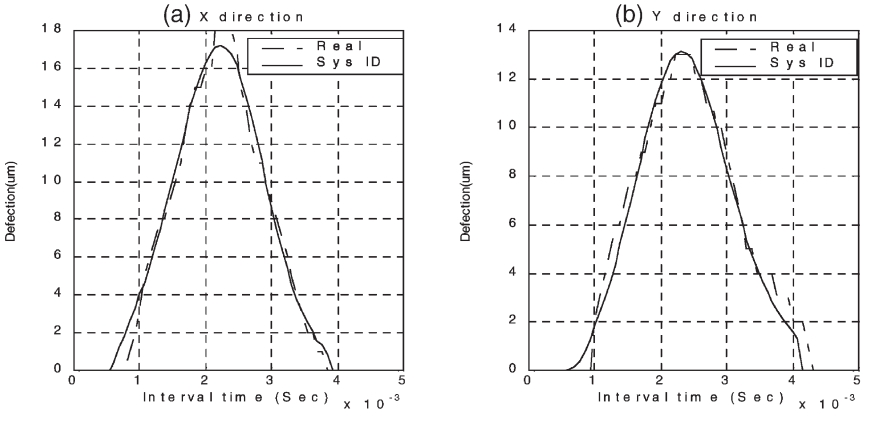


Fig. 14. Comparisons between real and identified table deflection.

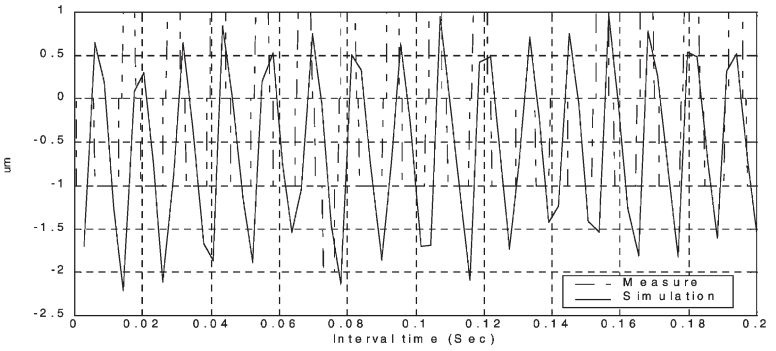


Fig. 15. Table displacements during cutting.

Table 2
Gains used in three controls for linear trajectory

| | $K_v$ | $K_{ex}$ | $K_{\varepsilon y}$ | $K_{ex}$ | $K_{ey}$ |
|---|---|---|---|---|---|
| US | 0 | 0 | 0 | 0.04 | 0.04 |
| CCS | 0 | 0.08 | 0.08 | 0.04 | 0.04 |
| CCPM | 0.01 | 0.08 | 0.08 | 0.04 | 0.04 |

Table 3
Gains in three controls for circular trajectory

| | $K_v$ | $K_{ex}$ | $K_{\varepsilon y}$ | $K_{ex}$ | $K_{ey}$ |
|---|---|---|---|---|---|
| US | 0 | 0 | 0 | 0.8 | 0.8 |
| CCS | 0 | 0.2 | 0.2 | 0.8 | 0.8 |
| CCPM | 0.4 | 0.2 | 0.2 | 0.1 | 0.1 |

which compares contour errors from three different controls when milling a circle of radius 10 mm. The uncoupled system (US), which performs tracking without cross-coupling compensation, yields the greatest absolute contour errors, but even if the cross-coupled (CCS) and the pre-compensated cross-coupled (CCPM) control can reduce the contour errors by an order of magnitude, the errors between pure tracking and tracking with cutting are significant (Fig. 16(a)–(c)).

Montgomery and Altintas [9] as well as Budak and Altintas [10] used cutting conditions to control cutting dynamics and achieve better surface roughness, but the approach of pure cutting ignores variation in the curvature of a workpiece profile; it is therefore susceptible to missing the best control activity. This fact can be understood by drawing the contour errors from Fig. 16 around a reference circle of radius 0.2 mm, as in Fig. 17. Clearly, the greatest contour errors occurred near 45° and 225° around the circle whichever of the three con-

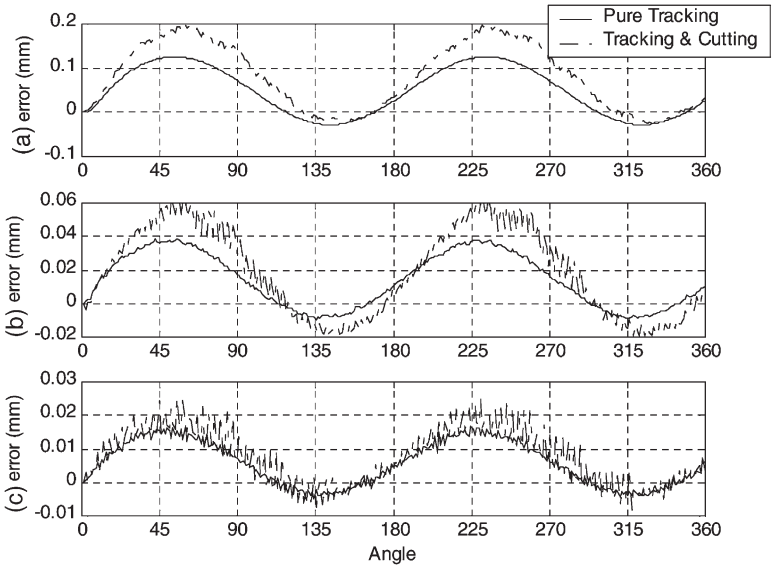


Fig. 16. Comparison of circular contour errors between pure tracking and tracking with cutting (a) US, (b) CCS, (c) CCPM (feed: 200 mm/s, *S*: 4800 rpm, axial depth of cut: 2 mm, radial depth of cut: 5 mm).

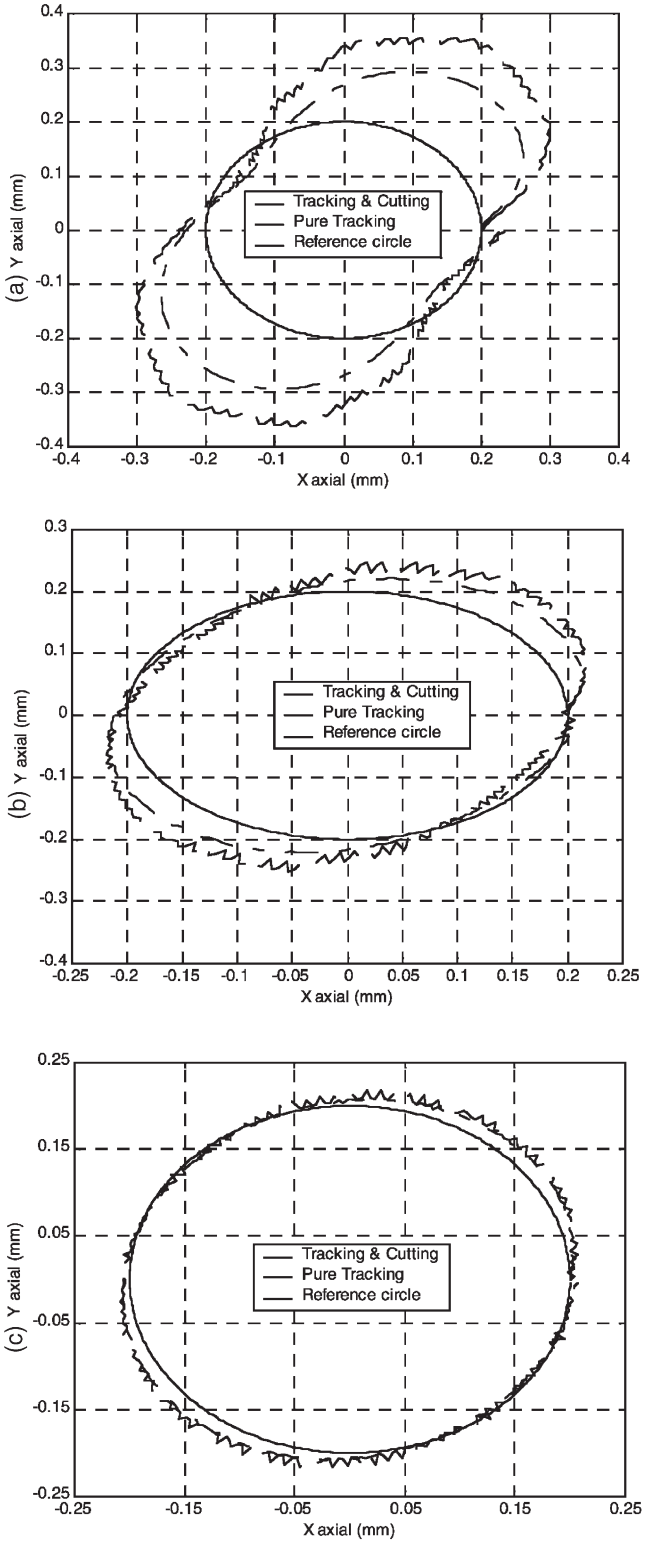


Fig. 17. Contour error as a function of angular position on a circle (a) US, (b) CCS, (c) CCPM (feed: 200 mm/s, *S*: 4800 rpm, axial depth of cut: 2 mm, radial depth of cut: 5 mm, reference circle = 0.2 mm).

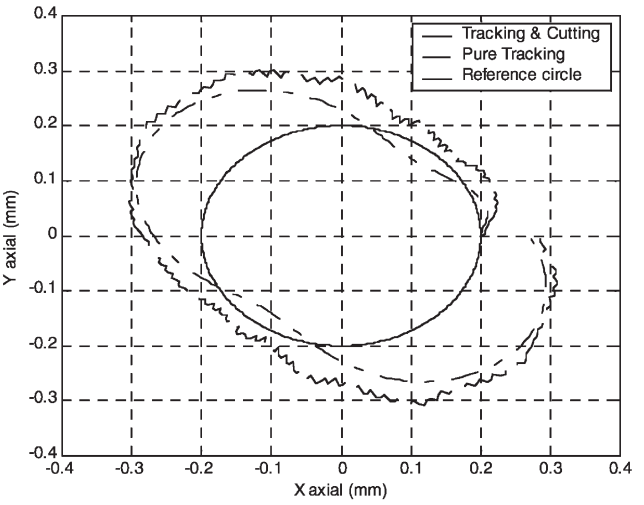


Fig. 18. Contour errors corresponding to Fig. 17(a) but with *x*- and *y*-axes motor dynamics exchanged.

trols were used. The cutting is not abnormal at these two locations; the errors are associated with trajectory and tracking, because at 45° and 225°, the trajectory undergoes the largest directional change and the *x*-axis motor has a lower time constant than the *y*-axis motor ($\tau_x < \tau_y$). Different feeding dynamics yield different results. Exchanging the motor time constants $\tau_x$ and $\tau_y$ yields the error results in Fig. 18. These trajectory or tracking bound contour errors can be better handled by trajectory planning or tracking than by manipulations of cutting conditions.

Another weakness associated with the pure consideration of cutting is embedded in the cutting force model. Usually, the cutting width is taken to be constant in most cutting force models [2,10]. However, in reality, the cut-

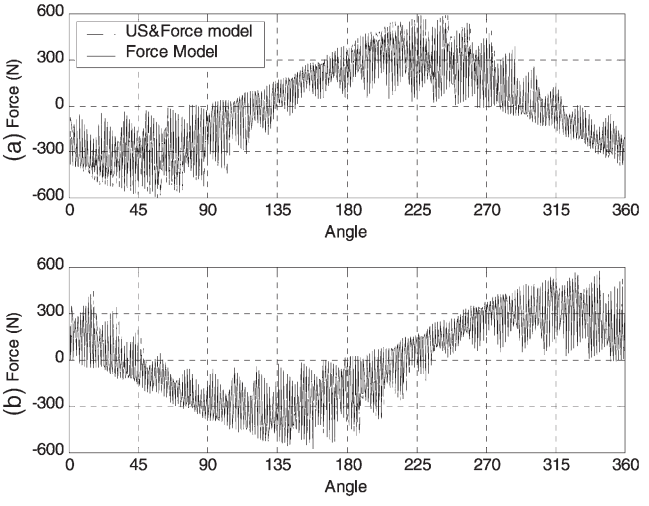


Fig. 19. Comparison of pure cutting force and cutting force during tracking of a circle with a diameter of 20 mm (a) *Fx*, (b) *Fy*; (feed: 200 mm/s, *S*: 4800 rpm, axial depth of cut: 2 mm, radial depth of cut: 5 mm).

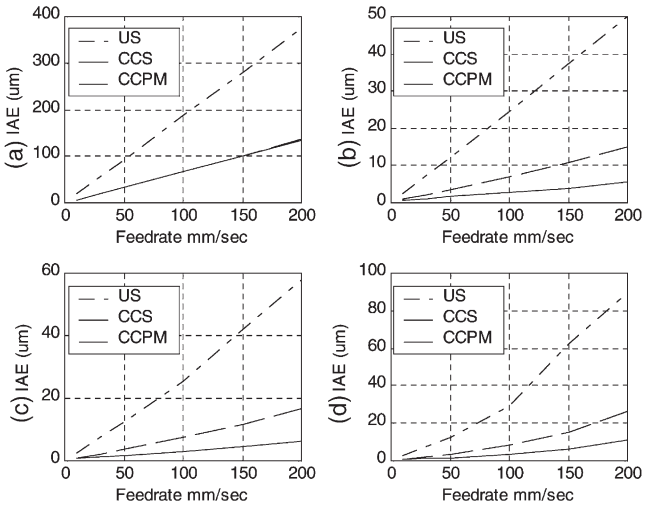


Fig. 20. Not cut: (a) linear 45, (b) *R* 30 mm, (c) *R* 10 mm, (d) *R* 5 mm.

ting width varies because of tracking activity, yielding a fluctuating "uncut chip" area, and a consequent variation in the cutting force not accounted for by the cutting force model. Fig. 19 shows the effect of feeding (trajectory tracking) on the cutting force. This figure pertains to the conditions of Fig. 16 to compare the cutting force model with and without feeding. The solid line in Fig. 19 represents the values predicted by the cutting force model, while the dotted line represents the values that result from the complete model. Fig. 19 reveals that the cutting force component *Fx* clearly differs from that predicted by the pure force model in the regions 30–90° and 210–270°, and that the *Fy* components differ in the regions 135–225° and 315–360°, because of the overcut or undercut of the trajectory (Fig. 16).

A series of simulations were performed to examine

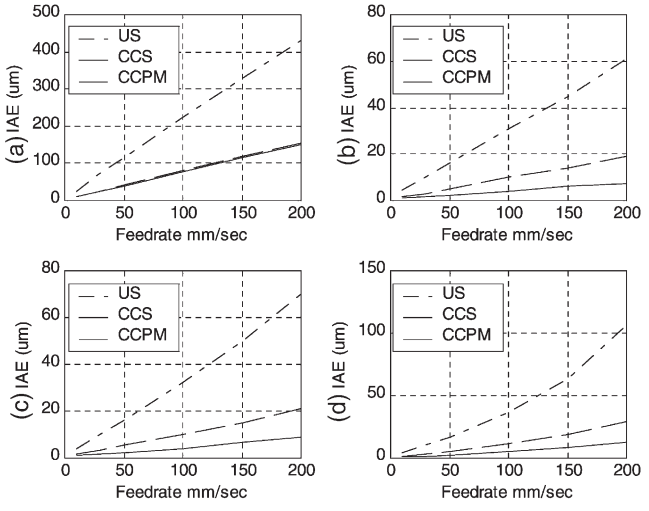


Fig. 21. Cut 0.5 mm: (a) linear 45, (b) *R* 30 mm, (c) *R* 10 mm, (d) *R* 5 mm.

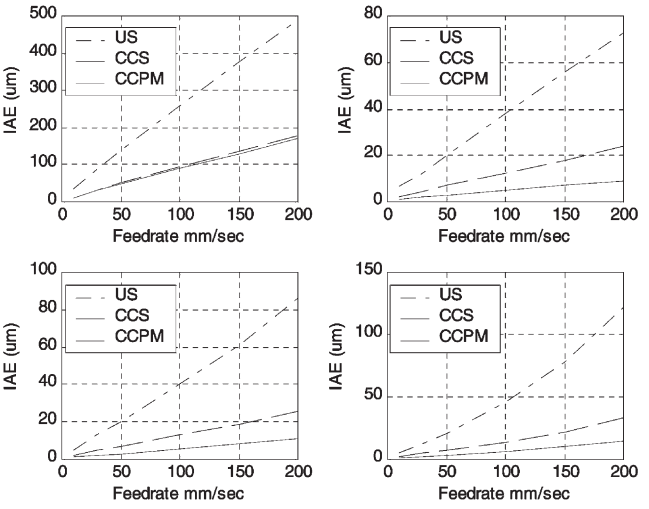


Fig. 22. Cut 1 mm: (a) linear 45, (b) *R* 30 mm, (c) *R* 10 mm, (d) *R* 5 mm.

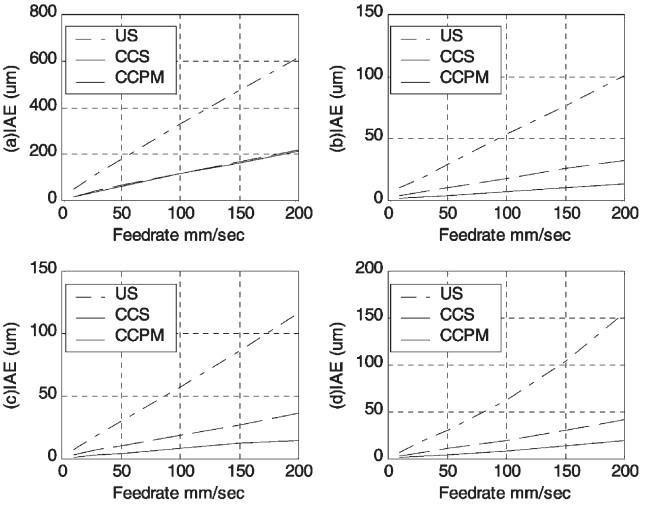


Fig. 23. Cut 2 mm: (a) linear 45, (b) *R* 30 mm, (c) *R* 10 mm, (d) *R* 5 mm.

the effect of the trajectory's curvature, feed-rate, cutting depth and different control on the complete CNC machining system, as depicted in Fig. 2.

Fig. 20 presents the "no cut" situation. In Figs. 21–23, the cutting conditions were as follows:

Cutting depth: 0.5, 1 and 2 mm;
Cutting width: 5 mm;
Trajectory: 45° linear path, circles of radius 30, 10 and 5 mm;
Feed-rate: 10, 30, 50, 100, 150, 200 mm/s;
Spindle speed: 4800 rpm.

Figs. 20–23 show that for straight-path machining, no difference exists between CCS and CCPM because no curvature is present to be crunched by CCPM. The contour error index varies roughly linearly with feed-rate at

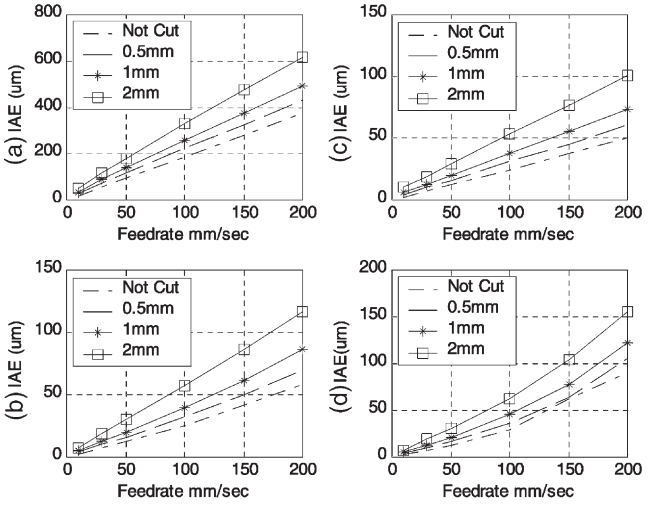


Fig. 24. (a) linear 45, (b) *R* 30 mm, (c) *R* 10 mm, (d) *R* 5 mm for US.

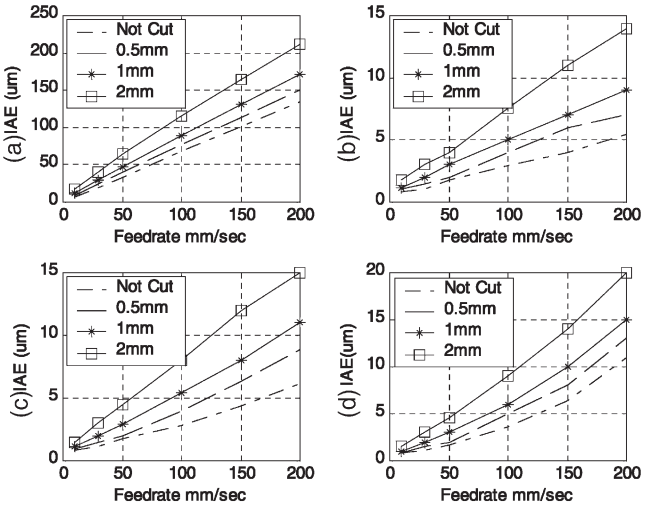


Fig. 26. (a) linear 45, (b) *R* 30 mm, (c) *R* 10 mm, (d) *R* 5 mm for CCPM.

low curvature, but tends to inflect upward at a higher curvature, and the CCPM better suppresses that tendency.

The cutting load is also observed to magnify the contour errors, as in Figs. 24–26, in which the cutting depth was considered explicitly to explicate its effect on contour errors for tracking without cross-coupled compensation (US), with cross-coupled compensation (CCS) and with pre-compensated, cross-coupled compensation (CCPM), respectively.

The core of generating a cutting force is the "uncut chip", whose size is determined by cutting depth and cutting width, the latter dependent on feed-rate in most cutting processes. Figs. 24–26 show that the contour error index increases linearly with feed-rate at no or moderate curvature, but parabolically at higher curvature (for example, at a radius 5 mm). Cutting depth intensifies the contour error index such that contour errors are larger at a higher feed-rate.

Notably, the examples presented in this work are "light cutting" because of the bench-top CNC milling machine available to perform the experiments. In heavy-duty cutting, the effect of cutting can be reasonably considered to be much larger.

Fig. 27 shows the effect of velocity pre-compensation provided by CCPM by comparing the absolute contour error index associated with CCS with that associated with CCPM. The comparisons verify that CCPM outperforms at higher curvature and higher feed-rate. However, the advantage of CCPM seems to diminish as the cutting

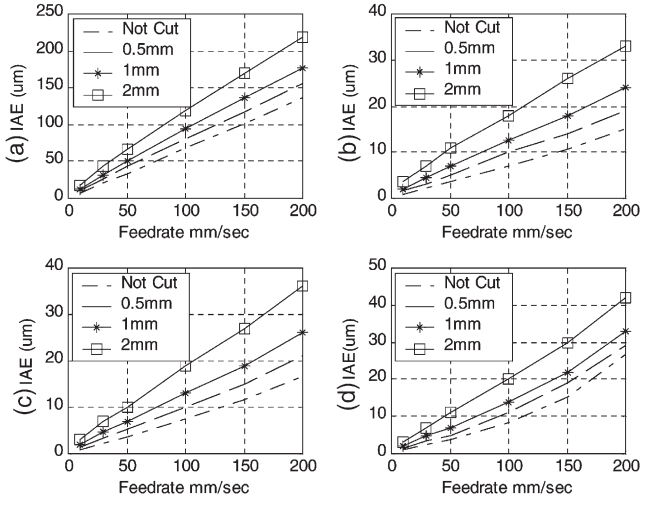


Fig. 25. (a) linear 45, (b) *R* 30 mm, (c) *R* 10 mm, (d) *R* 5 mm for CCS.

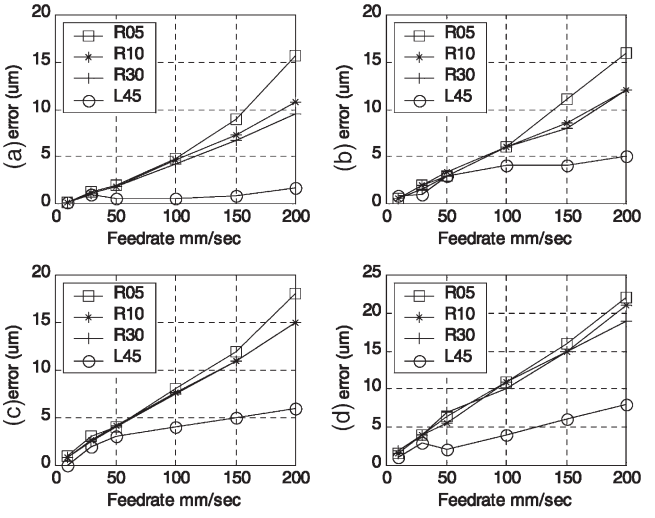


Fig. 27. CCS/iae-CCPM/iae: (a) Not cut, (b) 0.5 mm, (c) 1 mm, (d) 2 mm.

depth increases, implying that the cutting effect dominates and might eventually nullify the advantages of CCPM. This interesting phenomenon deserves further investigation in the future.

Fig. 28 elucidates the influence of cutting and feeding on the contour errors for a cutting depth of 1 mm and a spindle speed of 4800 rpm. It is seen that the contour errors are location phenomena; they become worse at certain trajectory locations and the cutting magnifies the errors differently at the different locations, suggesting that any attempt to improve the contour errors cannot overlook the trajectory features.

Using the data that generated Figs. 21–23 and the linear regression analysis function in Microsoft Excel allowed us to obtain the contributions of feed-rate, depth of cut and curvature to the contour errors under three different trajectory controls as follows

For US:

$$Er = 0.447 \times Fd + 14.022 \times Ad + 78.31 \times Cv - 22.67$$

For CCS:

$$Er = 0.129 \times Fd + 4.88 \times Ad + 16.2 \times Cv - 5.833$$

For CCPM:

$$Er = 0.53 \times Fd + 2.28 \times Ad + 9.62 \times Cv - 2.74.$$

where $Er$ represents the contour error (μm); $Fd$ is the feed-rate (mm/s), $Ad$ is the depth of cut (mm) and $Cv$ is the curvature ($mm^{-1}$).

In three cases, the ratio of coefficients $Cv$ and $Ad$ are 5.58, 3.32 and 4.22 for US, CCS and CCPM, respectively. The weights of the curvature and the depth of cut

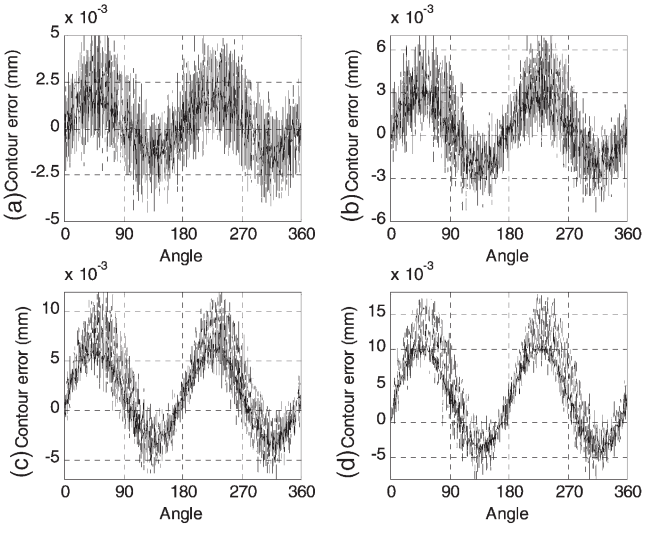


Fig. 28. Comparison of cut (red) and no cut (blue) in one spindle revolution at various feed-rates: (a) 10, (b) 30, (c) 50 and (d) 100 mm/s.

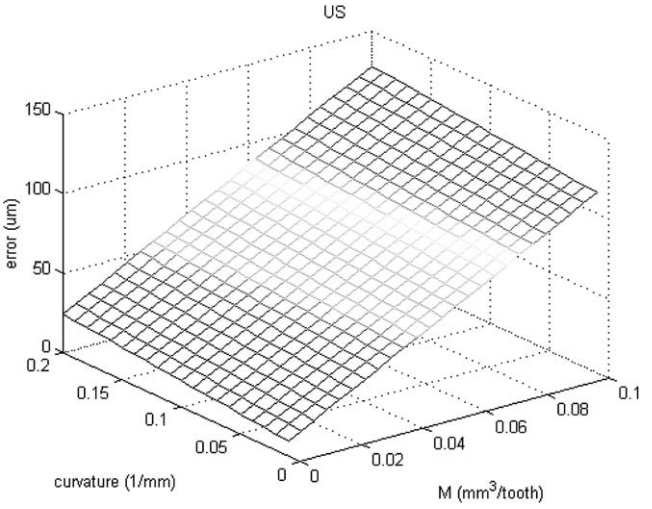


Fig. 29. Contour errors vs. curvature and metal removal per tooth for US.

on the contour errors are both sufficiently large. Negligence of any of which is inadequate.

To enable graphical representation, a parameter "metal removal per tooth" is calculated by multiplying the feed per tooth by the depth of the cut and the width of cut ($M$, $mm^3$/tooth). Figs. 29–31 show contour errors, determined by curvature and metal removal per tooth,for US, CCS and CCPM, respectively.

Notably, the metal removal per tooth includes contributions from feed-rate and cutting duty. Nevertheless, Figs. 29–31 indicate the dependency of contour errors on the curvature and the metal removal per tooth.

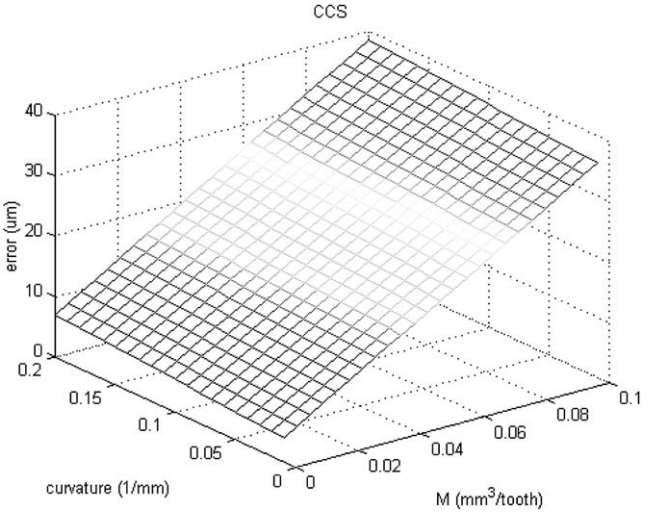


Fig. 30. Contour errors vs. curvature and metal removal per tooth for CCS.

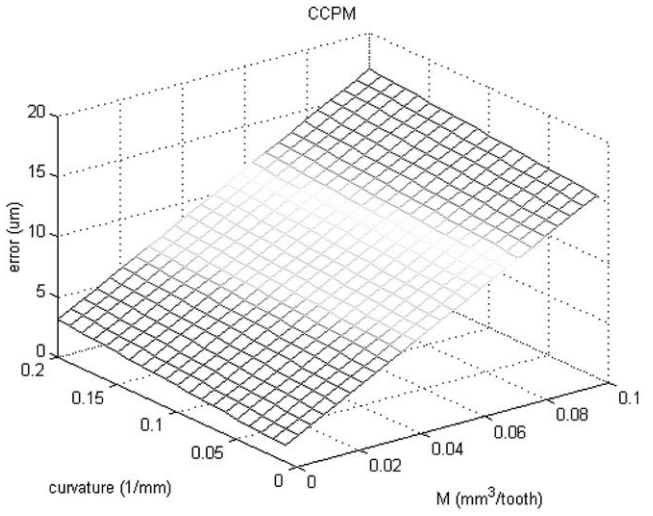


Fig. 31. Contour errors vs. curvature and metal removal per tooth for CCPM.

## 5. Conclusion

Modern CNC machines have two principal systems—the cutting system and the feeding system. Workpiece quality, no matter surface finish or contour accuracy, is the overall outcome of cutting and feeding systems. Previous studies have tended to approach CNC machining from the perspective of either cutting or feeding.

This work, however, investigated the contour errors on the basis of a complete CNC system. A system model that includes all groups of functions in CNC machining, namely trajectory planning, trajectory tracking, the cutting process, and the machine structure (spindle–tool structure and table structure) was established. Empirical data obtained for a table-top CNC milling machine were used to build the empirical cutting force model, the spindle–tool structure model and the table structure model. Contour errors were examined using this complete system.

The limitations of traditional studies were examined and discussed. According to our results, the approach that considers purely cutting suffers from ignoring the curvature-related features of the workpiece profile and the existence of tracking errors. Contour errors are local phenomena, and different errors occur at different locations on trajectory, so overlooking profile (trajectory) features makes the efforts of cutting controls inefficient. Besides, overlooking tracking errors is equivalent to assuming perfect feeding, hence leaving the variation of cutting forces and its consequences due to this cause unchecked.

Cutting was also shown to worsen contour errors in a manner that might eliminate some of the advantages gained by tracking techniques. This finding may lead to a re-thinking and re-developing of tracking strategies.

Some feeding and cutting parameters, including curvature, feed-rate, cutting depth and tracking control, were examined with reference to the proposed complete CNC machining system. It was found that contour errors increased with feed-rate, at a rate that escalates with curvature.

The approach proposed in this work represents a new way of understanding CNC machining.

## Acknowledgements

The authors would like to thank the National Science Council of the Republic of China, Taiwan for supporting this research under Contract No. NSC 90-2212-E-009-060.

## References

[1] M.E. Martelloti, An analysis of the milling process, Trans. ASME 63 (1941) 677.
[2] J. Tlusty, Dynamics of cutting forces in end milling, Ann. CIRP 24 (1975).
[3] Y.S. Tarng, C.I. Cheng, J.Y. Kao, Modelling of three-dimensional numerically controlled end milling operations, Int. J. Mach. Tools Manuf. 35 (7) (1995) 939–950.
[4] L. Zheng, Y.S. Chiou, S.Y. Liang, Three dimensional cutting force analysis in end milling, Int. J. Mech. Sci. 38 (3) (1996) 259–269.
[5] H.S. Kim, K.F. Ehmann, A cutting force model for face milling operations, Int. J. Mach. Tools Manuf. 33 (5) (1993) 651–673.
[6] P.J. Cheng, J.T. Tsay, S.C. Lin, A study on instantaneous cutting force coefficients in face milling, Int. J. Mach. Tools Manuf. 37 (10) (1997) 1393–1408.
[7] G. Yucesan, Y. Altintas, Prediction of ball end milling force, Trans. ASME, J. Eng. Ind. 118 (February) (1996) 95–103.
[8] J.W. Sutherland, R.E. DeVor, An improved method for cutting force and surface error prediction in flexible end milling system, Trans. ASME, J. Eng. Ind. 108 (November) (1986) 269–279.
[9] D. Montgomery, Y. Altintas, Mechanism of cutting force and surface generation in dynamic milling, Trans. ASME, J. Eng. Ind. 113 (May) (1991) 160–168.
[10] E. Budak, Y. Altintas, Peripheral milling conditions for improved dimensional accuracy, Int. J. Mach. Tools Manuf. 34 (7) (1994) 907–918.
[11] F. Ismail, M.A. Elbestawi, R. Du, K. Urbasik, Generation of milled surfaces including tool dynamics and wear, Trans. ASME, J. Eng. Ind. 115 (August) (1993) 245–252.
[12] P. Sarachik, J.R. Ragazzini, A two dimensional feedback control system, Trans. AIEE 76 (1957) 55–61.
[13] Y. Koren, Cross-coupled biaxial computer control for manufacturing, Trans. ASME, J. Dyn. Syst. Measur. Contr. 112 (1980) 225–232.
[14] Y. Koren, Variable-gain cross-coupling controller for contouring, Ann. CIRP 40 (1) (1991) 371–374.
[15] P.K. Kulkarni, K. Srinivasan, Cross-coupled control of biaxial feed drive servomechanisms, Trans. ASME, J. Dyn. Syst. Measur. Contr. 112 (1980) 265–272.
[16] J.H. Chin, J.C. Lin, Cross-coupled precompensation method for the contouring accuracy of computer numerically controlled machine tools, Int. J. Mach. Tools Manuf. 37 (7) (1997) 947–967.
[17] K. Erkorkmaz, Y. Altintas, High speed CNC system design. Part

III: high speed tracking and contouring control of feed drives, Int. J. Mach. Tools Manuf. 41 (2001) 1637–1658.
[18] X. Mei, M. Tsutsumi, T. Yamazaki, N. Sun, Study of the friction error for a high-speed high precision table, Int. J. Mach. Tools Manuf. 41 (2001) 1405–1415.
[19] The Fundamentals of Modal Testing, Application Note 243-3, Hewlett Packard, pp. 38–39.